# 145. Solution-Structure and Aggregation Behavior of Two Dilithiostyrene Derivatives[1])

by **Harald Günther*, Oswald Eppers, Heike Hausmann, Dietmar Hüls, Hans-Egbert Mons, Klaus-Dieter Klein**, and **Adalbert Maercker**

University of Siegen, Fachbereich 8, OC II, D-57068 Siegen

Dedicated to Professor Dr. *Wolfgang Lüttke* on the occasion of his 75th birthday

(13.IX.95)

The solution structure and the aggregation behavior of (*E*)-2-lithio-1-(2-lithiophenyl)-1-phenylpent-1-ene (**1**) and (*Z*)-2-lithio-1-(2-lithiophenyl)ethene (**2**) were investigated by one- and two-dimensional $^1$H-, $^{13}$C-, and $^6$Li-NMR spectroscopy. In $Et_2O$, both systems form dimers which show homonuclear scalar $^6$Li,$^6$Li spin-spin coupling. In the case of **2**, extensive $^6$Li,$^1$H coupling is observed. In tetrahydrofuran and in the presence of 2 mol of *N,N,N',N'*-tetramethylethylenediamine (tmeda), the dimeric structure of **1** coexists with a monomer. The activation parameters for *intra*-aggregate exchange in the dimers of **1** and **2** (**1** ($Et_2O$): $\Delta H^{\neq} = 62.6 \pm 13.9$ kJ/mol, $\Delta S^{\neq} = 5.8 \pm 14.0$ J/mol K, $\Delta G^{\neq}(263) = 61.1$ kJ/mol; **2** (dimethoxyethane): $\Delta H^{\neq} = 36.9 \pm 6.5$ kJ/mol, $\Delta S^{\neq} = -61 \pm 25$ J/mol K, $\Delta G^{\neq}(263) = 54.0$ kJ/mol) and the thermodynamic parameters for the dimer-monomer equilibrium for **1** ($\Delta H^{\circ} = 26.7 \pm 5.5$ kJ/mol, $\Delta S^{\circ} = 63 \pm 27$ J/mol K), where the monomer is favored at low temperature, were determined by dynamic NMR studies.

**Introduction.** – Modern NMR spectroscopy provides a number of 1D- and 2D-pulse sequences which have paved the way for extended and more detailed NMR investigations of organolithium compounds, in particular of systems which contain several nonequivalent Li-sites [2–6]. Apart from simple spin-echo spectroscopy [7] [8], 2D $^6$Li or $^7$Li-exchange spectroscopy (EXSY) [2], heteronuclear 1D $^1$H,$^6$Li- [9] or 2D [10] *Overhauser* measurements, and homo- as well as heteronuclear shift correlations of the $^6$Li,$^6$Li [11] and $^6$Li,$^{13}$C [12] type are of great importance. In favorable cases with regard to line width and relaxation behavior, even $^7$Li,$^7$Li-COSY [13] and $^1$H,$^7$Li-*Overhauser* measurements [14] could be performed. In addition, information about the aggregation states of organolithium compounds can be obtained from deuterium-induced isotope shifts of the $^6$Li-resonance [15].

In the following we report results from the application of a number of these NMR techniques to two $^6$Li-labelled dilithiostyrene compounds, (*E*)-2-lithio-1-(2-lithiophenyl)-1-phenylpent-1-ene (**1**) [16] and (*Z*)-2-lithio-1-(2-lithiophenyl)ethene (**2**; arbitrary numbering) [17]. These systems are related to (*E*)-1-lithio-2-(2-lithiophenyl)-1-phenylhex-1-ene (**3**), a dilithio compound formed by addition of butyllithium (BuLi) to tolane (1,1'-(1,2-ethynediyl)bis(benzene)) followed by metalation using a second mol of BuLi [18]. The solution structure of **3** was recently evaluated by a detailed NMR study [19]. With **2**, we

[1]) 'NMR Spectroscopy of Organolithium Compounds', Part XVIII; Part XVII: [1].

investigated the parent compound of the whole series of known dilithiostyrene systems, where the synthesis of other members with different substitution patterns is still in progress [20].

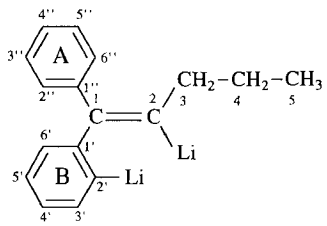

**1**

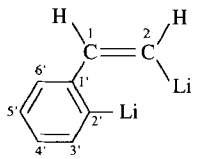

**2** (arbitrary numbering)

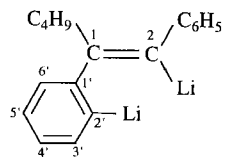

**3** (arbitrary numbering)

**Results.** – *Metalation Site in* **1** *and* **2**. Before starting to discuss the aggregation behavior of **1** and **2** in $(D_{10})Et_2O$, an unequivocal proof of the metalation sites was necessary; **1** was obtained by the reaction of Li-metal with (diphenylmethylidene)cyclobutane in $Et_2O$ *via* the short-lived intermediate **4** [16], while **2** precipitated from the reaction mixture of benzo[*b*]tellurophene (**5**) and BuLi in pentane/hexane [17], and was subsequently dissolved in $Et_2O$[2]).

The metalation sites in **1** and **2** were most easily established from the $^2$H-NMR spectra of the deuterolysis products, which show two signals, one in the aromatic and one in the olefinic region (*Fig. 1*). The Li-position in the aromatic ring then followed from the analysis of the $^1$H-NMR spectra of **1** and **2** (see below).

*Scheme*

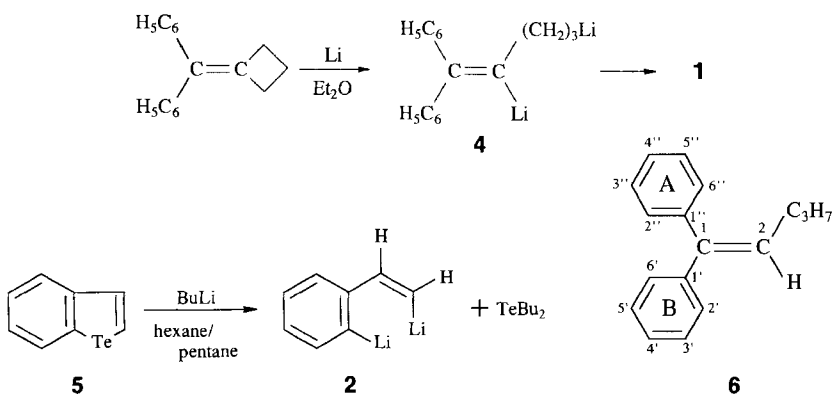

**5** **2** **6**

[2]) In the meantime, **2** was also prepared by lithiation of (*Z*)-2-lithiostyrene with BuLi/*N*,*N*,*N*′,*N*′-tetramethylethylenediamine (tmeda) [21].

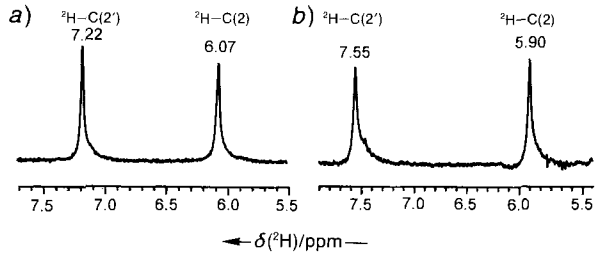


Fig. 1. *$^2$H-NMR Spectra of the deuterolysis products from* a) **1** *and* b) **2**

For **1**, a more intriguing problem was posed by the question which of the two Ph rings is metalated. This question was solved by combining the results of the analysis of the $^1$H-NMR spectrum of the hydrolysis product, 1,1-diphenylpent-1-ene (**6**), with those of a 2D nuclear *Overhauser* (NOESY) [22] [23] experiment.

The 400-MHz $^1$H-NMR spectrum of **6** (*Fig. 2, a, b*) displays a fairly well resolved *ABB'CC'* spin system for one Ph ring, which was analyzed (*Fig. 2c*). The remaining signals in the region $\delta$ 7.20–7.25 must then belong to the strongly coupled five-spin system of the second Ph ring. Since the NOESY spectrum of **6** (*Fig. 3*) established spatial proximity of the olefinic proton H–C(2) and the protons which give rise to these resonances, these signals were identified as belonging to ring B. Consequently, because the $^2$H-signal in the aromatic region of $D_2$-**6** (*cf. Fig. 1, a*) coincides with these $^1$H-signals, metalation had occurred in ring B, and the well-resolved $^1$H-subspectrum in the aromatic region must be assigned to ring A.

The assignment derived for the $^1$H-NMR spectrum of **6** was supported by a heteronuclear $^{13}$C,$^1$H-shift correlation which disclosed the multiplicities for the $^1$H-signals of both rings most clearly (*Fig. 4*). It established that two resonances with a *t* and a *d* structure, respectively, (*H*–C(2')/*H*–C(6') and H–C(3')/H–C(5')) are nearly degenerate at $\delta$ 7.23 and demonstrated again the power of the 2D method where overlapping signals are separated in the second frequency dimension. The complete $^1$H- and $^{13}$C-NMR data for **6** are given in *Tables 1* and *2*.

*$^1$H-, $^{13}$C-, and $^6$Li-NMR Spectra of* **1** *and* **2**. The $^1$H-NMR spectra (*Fig. 5*), recorded at room temperature, show the expected low-field absorption of H–C(3'), the aromatic proton in *ortho*-position to the metal. For **2**, deshielding was also found for the resonance of H–C(1) and H–C(2). The assignment of the remaining resonances was established by standard $^1$H,$^1$H-COSY-45 and NOESY experiments [23] (see *Exper. Part*).

After the $^1$H-NMR spectra had been assigned and analyzed (*Table 1*), whereby extensive $^6$Li,$^1$H coupling was found for **2** which required $^6$Li-decoupling for the analysis, the $^{13}$C-NMR spectra were assigned by $^{13}$C,$^1$H-shift correlations based on one-bond and long-range $^{13}$C,$^1$H-coupling constants (HETCOR and HMQC experiments [23], resp.; see *Exper. Part*). The long-range experiments (room temperature) provided the assignment of all quaternary C-atoms and established also the metalated-C resonances (*Table 2*) with values of 187.4 and 177.7 ppm for C(2) and 172.2 and 173.1 ppm for C(2') in **1** and **2**, respectively.

Two signals of equal intensity were observed at 223 K for **1** in the $^6$Li-NMR spectra, which were assigned by 1D $^6$Li$\{^1$H$\}$-NOE difference spectroscopy. As *Fig. 6, a* demonstrates, irradiation of the $CH_2$ protons of the propyl (Pr) group, respectively, yields an *Overhauser* enhancement for the high-field $^6$Li-signal, while irradiation of the aromatic H–C(3') yields the *Overhauser* enhancement at low field. In the case of **2**, two

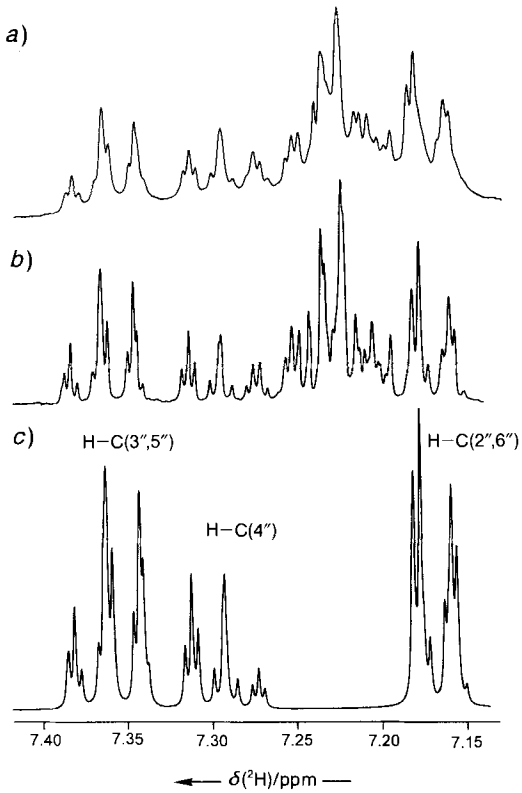


Fig. 2. *400-MHz $^1$H-NMR Spectra of* **6**: a) *experimental spectrum of the hydrolysis product from* **1**; b) *authentic sample of* **6** *obtained by independent synthesis*; c) *calculated spectrum for the Ph protons of ring A of* **6**

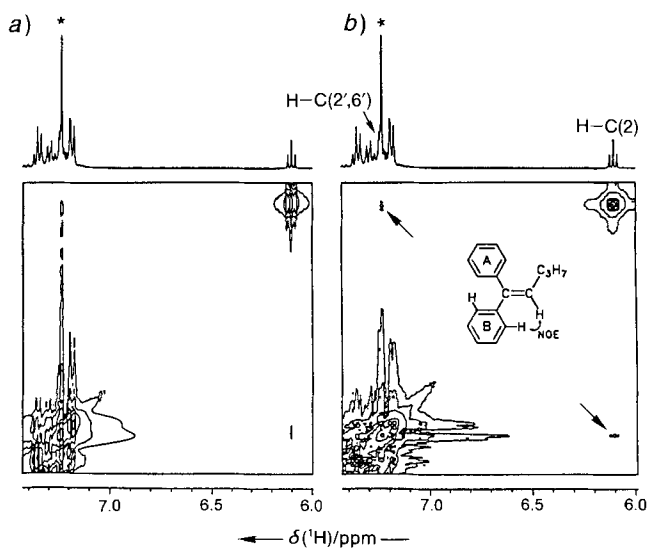


Fig. 3. *$^1$H-NOESY Spectra of* **6**: a) *unsymmetrized*; b) *symmetrized*

Table 1. *$^1$H-NMR Data* ($\delta$ [ppm] rel. to $SiMe_4$, $J$ [Hz]) *of* **1** (**7a**), **2** (**7b**), *and* **6** *at 298 K*

| | H–C(1) | H–C(2) | H–C(2′) | H–C(3′) | H–C(4′) | H–C(5′) | H–C(6′) | H–C(2″,6″) | H–C(3″,5″) | H–C(4″) | $CH_2$(3) | $CH_2$(4) | Me(5) |
|---|---|---|---|---|---|---|---|---|---|---|---|---|---|
| **1** | – | – | – | 7.996 | 6.833 | 6.880 | 6.780 | 7.077 | 7.308 | 7.139 | 2.23 | 1.36 | 0.79 |
| **2** | 8.48 | 7.17 | – | 7.96 | 6.84 | 7.01 | 7.10 | – | – | – | – | – | – |
| **6** | – | 6.07 | [a]) | [a]) | [a]) | [a]) | [a]) | 7.16 | 7.35 | 7.29 | 2.09 | 1.44 | 0.91 |

| | $J$(1,2) | $J$(3′,4′) | $J$(3′,5′) | $J$(3′,6′) | $J$(4′,5′) | $J$(4′,6′) | $J$(5′,6′) | r.m.s.[b]) | $J$(2″,3″) = $J$(5″,6″) | $J$(2″,4″) = $J$(4″,6″) | $J$(2″,5″) = $J$(3″,6″) | $J$(2″,6″) | $J$(3″,4″) = $J$(4″,5″) | $J$(3″,5″) | r.m.s.[b]) |
|---|---|---|---|---|---|---|---|---|---|---|---|---|---|---|---|
| **1** | – | 6.91 | 1.67 | 0.27 | 6.99 | 0.95 | 7.66 | 0.06 | 7.78 | 1.22 | 0.42 | 1.77 | 7.14 | 1.40 | 0.03 |
| **2** | 16.97 | 6.70 | 1.57 | 0.71 | 7.19 | 1.14 | 7.65 | 0.01 | – | – | – | – | – | – | – |
| **6** | – | [a]) | [a]) | [a]) | [a]) | [a]) | [a]) | | 7.67 | 1.24 | 0.62 | 1.63 | 7.48 | 1.31 | 0.07 |

Long-range coupling to the aromatic ring of **2**: $J(1,6') = 0.5$, $J(1,3') = 0.6$, $J(2,6') = 0.2$, $J(2,5') = 0.2$, $J(1,4') = 0.1$, $J(2,4') = 0.2$

[a]) Not resolved, *m* from 7.18 to 7.25 ppm.

[b]) Standard deviation (root-mean-square value) between calculated and experimental line frequencies.

Table 2. *$^{13}$C-NMR Chemical Shift Data* ($\delta$ [ppm] rel. to $SiMe_4$) *of* **1a** (**7a**, **8a**), **2** (**7b**), **3**[a]), *and* **6** *and* $^1J(C,H)$ *Data* [Hz] *for* **2** (**7b**) *at 298 K*

| | C(1) | C(2) | C(1′) | C(2′) | C(3′) | C(4′) | C(5′) | C(6′) | C(1″) | C(2″,6″) | C(3″,5″) | C(4″) | C(3) | C(4) | Me(5) | Solvents |
|---|---|---|---|---|---|---|---|---|---|---|---|---|---|---|---|---|
| **7a** | 158.1 | 187.4 | 157.1 | 172.2 | 143.6 | 123.5 | 126.9 | 128.8 | 147.8 | 130.3 | 128.3 | 125.1 | 43.9 | 26.9 | 15.5 | $Et_2O$ |
| **7a** | | 186.9 | | 174.0 | | | | | | | | | | | | THF |
| **8a**·tmeda | | 204.2 | | 186.3 | | | | | | | | | | | | THF |
| **7b**[b]) | 156.6 | 177.7 | 156.2 | 173.1 | 144.7 | 124.0 | 126.5 | – | – | – | – | – | – | – | – | $Et_2O$ |
| $\mathbf{3}_2$ (dimer) | 150.8 | 190.2 | 154.9 | 175.9 | 143.4 | 123.3 | 126.6 | 124.3 | 161.3 | 123.3 | 128.2 | 119.3 | | | | THF |
| **3**·tmeda | 144.7 | 202.1 | 154.8 | 189.5 | 143.7 | 121.9 | 124.9 | 121.7 | 163.8 | 121.7 | 127.8 | 116.6 | | | | THF |
| **6** | 141.6 | 130.0 | 142.9 | 127.2 | 128.0 | 126.7 | 128.0 | 127.2 | 140.3 | 129.9 | 128.1 | 126.8 | 31.8 | 23.1 | 13.8 | |

[a]) From [19].

[b]) $^1J(C(1),H) = 141.0$, $^1J(C(2),H) = 104.5$, $^1J(C(3'),H) = 151.6$, $^1J(C(4'),H) = 154.5$, $^1J(C(5'),H) = 156.2$, and $^1J(C(6'),H) = 150.0$ Hz.

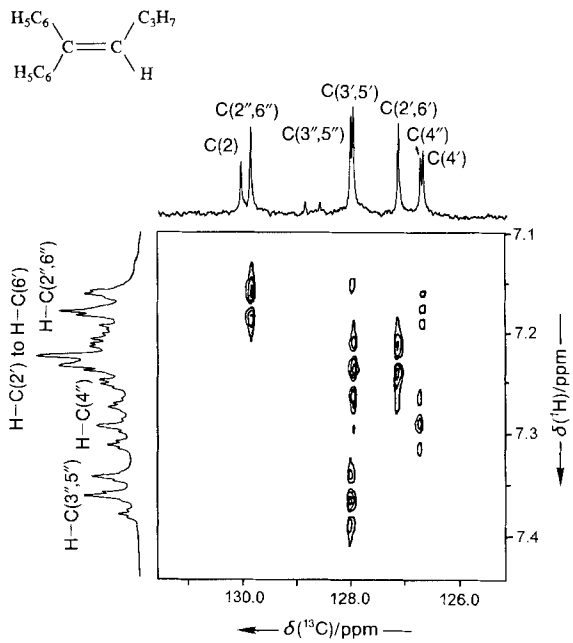


Fig. 4. *100/400-MHz $^{13}C,^{1}H$-Shift correlation for the Ph protons of* **6**

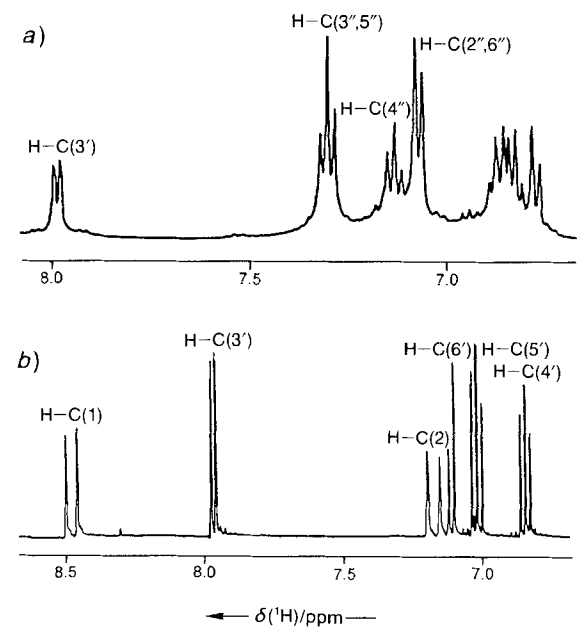


Fig. 5. *400-MHz $^{1}H$-NMR Spectra of* a) **1** *and* b) **2** *at 298 K*

$^6$Li-NMR signals are already found at room temperature (*Fig. 6, b*). Here, the correlation between H–C(3′) and the low-field $^6$Li-signal as well as between H–C(2) and the high-field $^6$Li-signal was established by a two-dimensional $^1$H,$^6$Li-HOESY experiment [10] (*Fig. 6, b*). In both compounds, therefore, the Li close to the olefinic C-atom resonates at high field, while the Li close to the aromatic C-atom resonates at low field.

*Aggregation Behavior of* **1** *and* **2** *in* $Et_2O$. After having established the structure of the building blocks of the new polylithium systems, their aggregation state could be investigated. The observation of only one set of signals in the $^1$H- as well as in the $^{13}$C-NMR spectra, also in the low-temperature region where *intra*- and *inter*-aggregate exchange processes are slow, demonstrated that a single aggregate was present for **1** and **2** in $Et_2O$. Reasonable structural alternatives are the dimer **7** and the monomer **8**, analogous to the structures found for the aggregates of **3** in THF [19]. We will show below that a dimeric structure must be assigned to **1** and **2** in $Et_2O$.

Arguments in favor of **7** were obtained from the $^6$Li,$^6$Li-INADEQUATE spectra (*Fig. 7*), which demonstrated homonuclear spin-spin coupling between the two $^6$Li-resonances detected in the $^6$Li-NMR spectrum. This fact is only compatible with the dimer where both nonisochronous $^6$Li-nuclei reside in the same cluster. For a monomer **8** with a double Li-bridge, both Li-nuclei are isochronous and a $^6$Li *s* is expected (see below). An even more direct proof was possible for **2**, where low-temperature measurements under

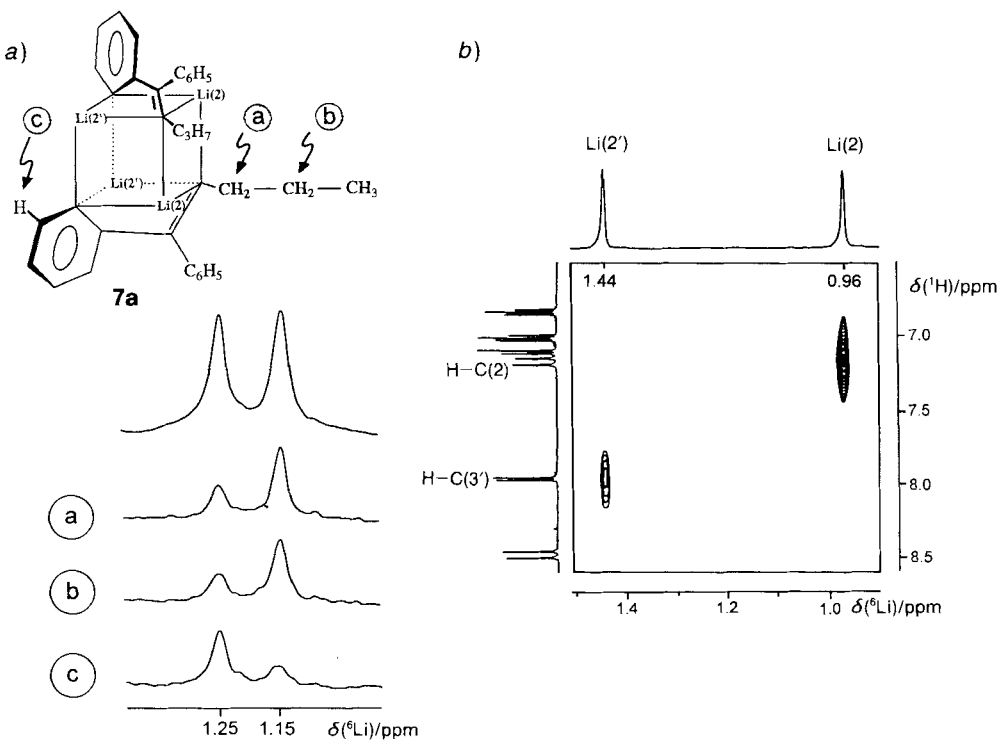


Fig. 6. a) *1D-NOE Experiments for* **1**(**7a**) (223 K); b) *2D-HOESY spectrum of* **2** (**7b**) (298 K)

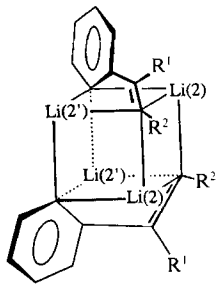


**7a** $R^1 = Ph$, $R^2 = Pr$
**b** $R^1 = R^2 = H$

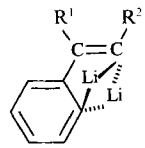


**8a** $R^1 = Ph$, $R^2 = Pr$
**b** $R^1 = R^2 = H$

heteronuclear $^1H$- and homonuclear $^6Li$-decoupling revealed four different $^6Li$-resonances of equal intensity [24]. Thus, the dimer **7b** has only $C_1$ symmetry.

Independent information regarding structure **7** was available through the application of the isotopic fingerprint method [15]. For this purpose, the partially deuteriated building blocks **9** and **10** were synthesized from suitably deuteriated precursors (see *Exper. Part*). A 1:1 mixture **1**/**9** yielded at 169 K the spectrum shown in *Fig. 8, a*, with a *t* for Li(2') (environments: ***h***,***h***; ***h***,***d*** = ***d***,***h***; ***d***,***d***)[3]) and a *d* for Li(2) (environments ***h*** or ***d***). This confirms the dimeric structure **7a**.

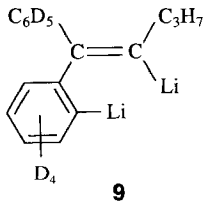


**9**

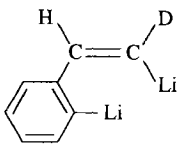


**10**

In the case of the 1:1 mixture **2**/**10**, the $^6Li$-spectra shown in *Fig. 8, b–d*, were recorded. A *t* is now expected for Li(2) coordinated to the olefinic C-atom and a *d* for Li(2'). Experimentally, two broadened resonances were found (*Fig. 8, d*), which both yielded a *t* structure only upon $^1H$- and homonuclear $^6Li$-decoupling (*Fig. 8, b, c*). This unexpected result is caused by the fact that for the Li(2') resonance, two closely spaced lines were observed [24]. Under conditions of homonuclear decoupling, the two nonequivalent Li(2') resonances were separated at room temperature by 0.17 Hz or 2.9 ppb, which is in the order of the $^2H/^1H$-NMR isotope shift. The shift separation for Li(2), on the other hand, was only observed at lower temperature. Thus, the '*t*' recorded for the $^6Li(2')$ resonance in the 1:1 mixture **2**/**10** is in fact a *dd*, and this is in agreement with the dimeric structure **7b**.

---

[3]) ***h*** = non-deuteriated ligand; ***d*** = deuteriated ligand.

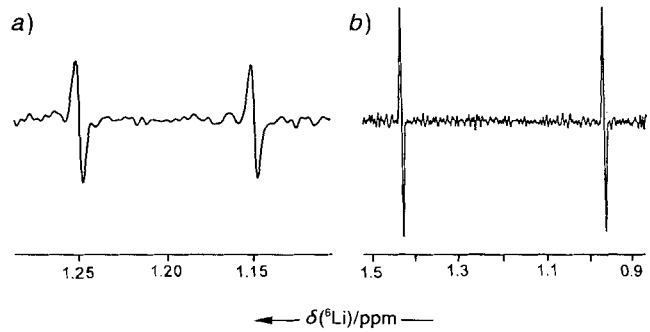


Fig. 7. *$^6$Li,$^6$Li-INADEQUATE Spectra of* a) **1** (**7a**) (203 K) *and* b) **2** (**7b**) (298 K)

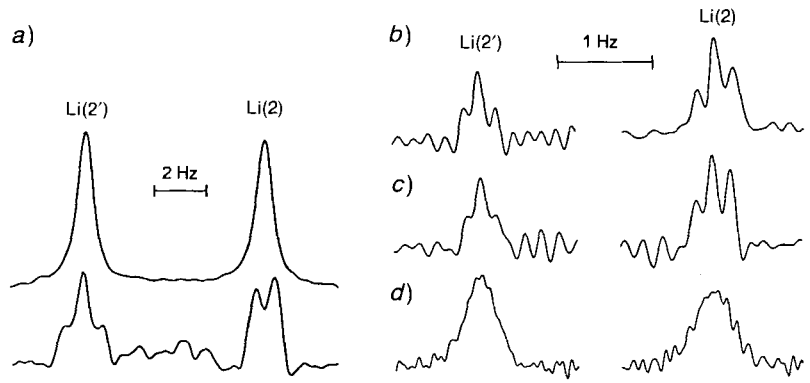


Fig. 8. *$^6$Li-NMR Spectra of* a) **1** (above) and **7a**/$D_5$-**7a** (below) (169 K) *and* b)–d) **7b**/*D*-**7b** (298 K)

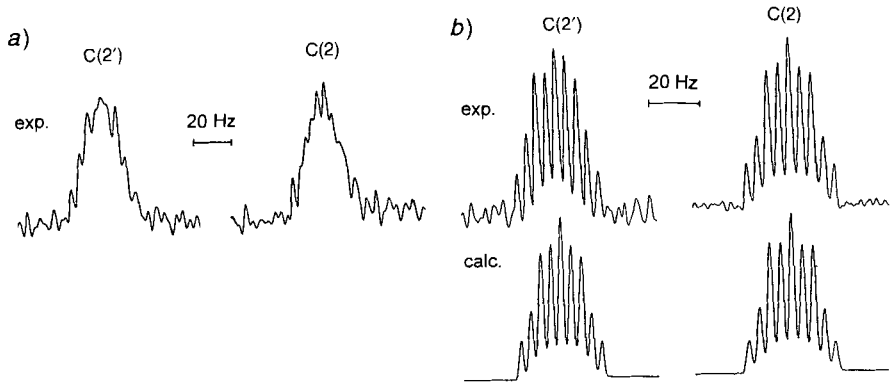


Fig. 9. *$^{13}$C-NMR Multiplets for the lithiated C-atoms of* a) **7a** (181 K) *and* b) **7b** (298 K) *in* $Et_2O$

Finally, the inspection of the $^{13}C,^{6}Li$-coupling constants clearly demonstrated that each metalated C-atom is coordinated to at least two different Li-atoms. The *m*'s of C(2) and C(2') (*Fig. 9*) immediately indicated by their complex splitting pattern that several nonequivalent $^{13}C,^{6}Li$-coupling constants are present. For **2**, these parameters were determined by spectral simulation of the $^{13}C$-pattern as well as by the observation of the $^{13}C$-satellites in the $^{6}Li$-NMR spectrum which was essential for an unequivocal assignment. These results are collected in *Table 3*. A similar analysis for **1** was so far hampered by line-broadening effects which prevented the satellite observation.

Table 3. *$^{13}C,^{6}Li$-Coupling Constants* [Hz] *for* **7b**

| | *J*(C(2'),Li(2')) | *J*(C(2'),Li(2)) | *J*(C(2),Li(2')) | *J*(C(2),Li(2)) |
|---|---|---|---|---|
| $^{6}Li$-NMR[a]) | 4.3 | 8.2 | 7.9 | 3.7 |
| $^{13}C$-NMR[b]) | 3.7, 4.5 | 8.2 | 8.8 | 4.3, 4.5 |

[a]) From $^{13}C$-satellite measurements in the $^{6}Li$-NMR spectrum.
[b]) From spectral simulation of the $^{13}C$-NMR signal.

*Aggregation States of* **1** *in Tetrahydrofuran (THF) in the Presence of* N,N,N',N'-*Tetramethylethylenediamine* (tmeda). The formation of a monomeric species **8a** in THF/tmeda in addition to the dimer **7a** was already reported [25]. A 1D $^{6}Li,^{6}Li$-INADEQUATE experiment served to distinguish the $^{6}Li$-NMR *s* ($\delta$ 1.45 rel. to 0.1M LiBr in THF) from the $(AX)_2$ system of the dimer ($\delta(^{6}Li)$ 1.53 and 1.82 ppm) shown below in *Fig. 14*. In *Fig. 10*, we show the $^{13}C$-NMR signals for the metalated C-atoms of the dimer (d)/monomer (m) mixture where, in addition to the dimer resonances (see *Fig. 9a*), two well resolved *quint.* at 204.2 and 186.3 ppm with a splitting of $J(C,Li) = 10.3 \pm 1.3$ and $6.7 \pm 0.3$ Hz, respectively, were observed for the monomer.

*Dynamic Behavior of the Dimers* **7a** *and* **7b**. Cross-peaks were observed in the $^{6}Li$-2D-EXSY spectrum of **7a** at 230 K which demonstrate chemical exchange for the Li-nuclei, and the temperature-dependent line shape of the 1D-$^{6}Li$-NMR spectrum is shown in *Fig. 11*. Assuming a first-order exchange reaction for this process, the experimental spectra were simulated on the basis of the *Gutowsky-Holm* theory [26] to obtain first-order rate constants (*cf. Exper. Part*). The line-shape analysis yielded the following

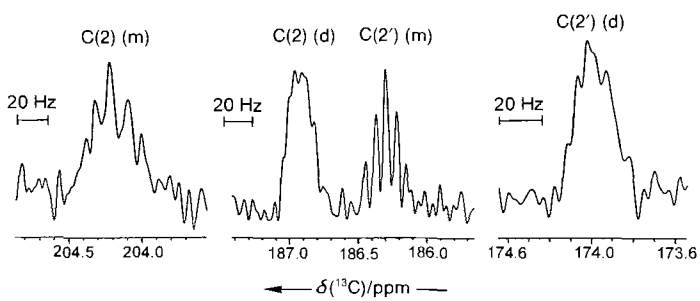


Fig. 10. *$^{13}C$-NMR Multiplets for the lithiated C-atoms of* **7a** (d = dimer) *and* **8a** · *2tmeda* (m = monomer) *in THF*

activation parameters: $\Delta H^{\neq} = 62.6 \pm 13.9$ kJ/mol, $\Delta S^{\neq} = 5.8 \pm 14.0$ J/mol K, and $\Delta G^{\neq} = (263)\ 61.1$ kJ/mol. A unique feature of the $^6$Li-NMR spectrum is the temperature dependence of the chemical-shift difference $\delta\nu$ which decreases after decoalescence in the slow-exchange limit. At 253 K, both $^6$Li signals coincide, and below this temperature, $\delta\nu$ increases again. This behavior can only be explained by a different temperature gradient for both Li-sites with the crossover point around 253 K.

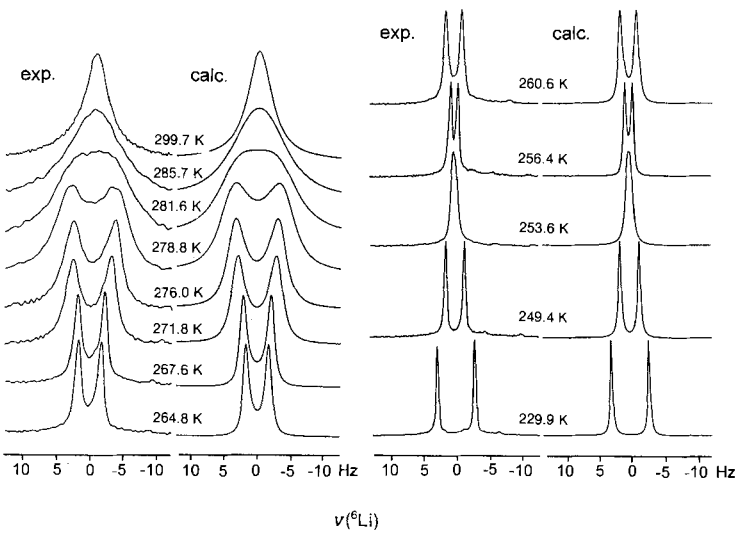


Fig. 11. *Temperature dependence of the $^6$Li-NMR spectrum of* **7a**

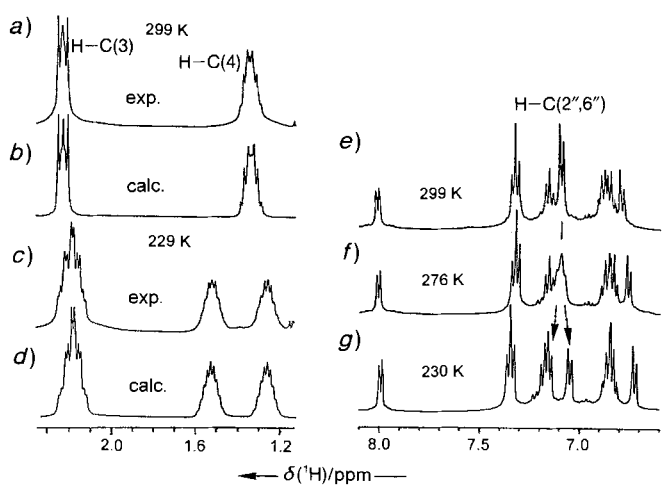


Fig. 12. *Temperature dependence of the $^1$H-NMR spectrum of* **7a**: a)–d) *propyl region*; e)–g) *aromatic region*

In addition to the $^6$Li-NMR study, the temperature dependence of the $^1$H-NMR spectrum of **7a** in $Et_2O$ was investigated. Two interesting aspects emerged from these measurements: *1*) The spectrum of the Pr group changes from an $AA'MM'X_3$ system at 299 K to an $ABKMX_3$ system at 229 K, and the *ortho*-protons of the Ph ring B (H–C(2″,6″)) show line splitting in the same temperature range and display nonequivalent signals at 230 K (*Fig. 12*). From the coalescence phenomena in the $^1$H-NMR spectrum, activation barriers of $\Delta G^{\neq}(276) = 58.7$ (from H–C(3)), $\Delta G^{\neq}(294) = 58.5$ (from H–C(4)), and $\Delta G^{\neq}(276) = 59.9$ kJ/mol (from H–C(2″,6″)) are derived. The $^1$H-NMR parameters of the Pr groups, given in *Table 4*, were estimated from a non-iterative line-shape simulation at two different temperatures.

Table 4. *NMR Parameters* $\delta$ [ppm] *and* J [Hz] *of the Propyl Groups in* **7a** *at Two Different Temperatures* (*cf. Fig. 11*)

| | 229 K | 299 K | | 229 K | 299 K |
|---|---|---|---|---|---|
| Spin system | $ABKMX_3$ | $AA'BB'X_3$ | $J(3,3')$ | –12.1 | –10.8 |
| $\delta$(Me(5)) | 0.782 | 0.757 | $J(3,4)$ | 4.6 | 4.9 |
| $\delta$(H–C(3)) | 2.173 | 2.218 | $J(3,4')$ | 12.6 | 11.8 |
| $\delta$(H′–C(3)) | 2.222 | 2.218 | $J(4,4')$ | –11.8 | –10.7 |
| $\delta$(H–C(4)) | 1.256 | 1.346 | | | |
| $\delta$(H′–C(4)) | 1.526 | 1.346 | | | |

For **7b**, three different solvents were used to study exchange processes: $Et_2O$, THF, and dimethoxyethane (glyme). In all solvents, the $^6$Li-NMR spectrum displayed two signals, and no indication of a third signal belonging to a monomer was found. Variation of the temperature did show small chemical-shift changes but no line-broadening effects in $Et_2O$. In THF, coalescence was indicated at *ca.* 300 K, and in glyme it was measured at 263 K. From these temperatures and the experimental chemical-shift differences, the following $\Delta G^{\neq}$ values (in kJ/mol) can be estimated: > 63 ($Et_2O$, 300 K), *ca.* 63 (THF, 300 K), and 54 (glyme, 263 K). A line-shape analysis of the temperature-dependent $^6$Li-spectrum in glyme (*Fig. 13*) yielded $\Delta H^{\neq} = 36.9 \pm 6.5$ kJ/mol and $\Delta S^{\neq} = -61 \pm 25$ J/mol K.

*Monomer-Dimer Equilibrium* **8a** $\rightleftharpoons$ **7a**. From the $^6$Li-NMR spectra shown in *Fig. 14*, it was possible to calculate the monomer and dimer concentrations and the equilibrium constant $K$ from the measured line intensities obtained by integration (see *Exper. Part*). As in the case of **3** $\rightleftharpoons$ $\mathbf{3}_2$ (monomer $\rightleftharpoons$ dimer) [19], the following equilibrium was assumed: 2(**8a**·2tmeda) + 4 THF $\rightleftharpoons$ **7a**·4 THF + 4tmeda. A *van't Hoff* plot then yielded $\Delta H^{\circ} = 26.7 \pm 5.5$ kJ/mol and $\Delta S^{\circ} = 63 \pm 27$ en.

**Discussion.** – *Structure and Dynamics.* As our results show, the structurally related systems **1** and **3** not unexpectedly behave largely similarly. Both form dimers and monomers, and the kinetic parameters for the dynamic process which leads to coalescence of the $^6$Li-signals in the dimer are of comparable magnitude: $\Delta G^{\neq}(263) = 61.1$ and 66.1 kJ/mol for **1** and **3**, respectively. Again, as in the case of **3**, nearly identical barriers (58.5–59.9 kJ/mol) are found for the dynamic processes in the $^1$H-NMR spectra of **7a**, which characterize the observed loss of diastereotopicity for the $CH_2$ protons of the Pr groups and the aromatic *ortho*-protons of ring A.

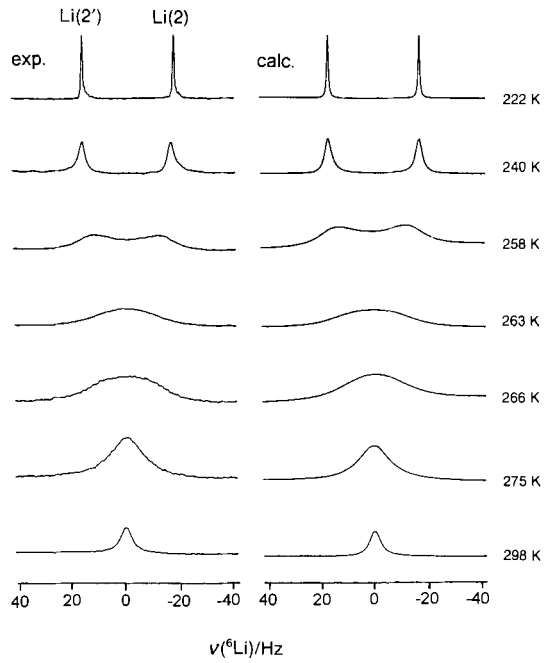


Fig. 13. *Temperature dependence of the $^{6}$Li-NMR spectrum of* **7b**

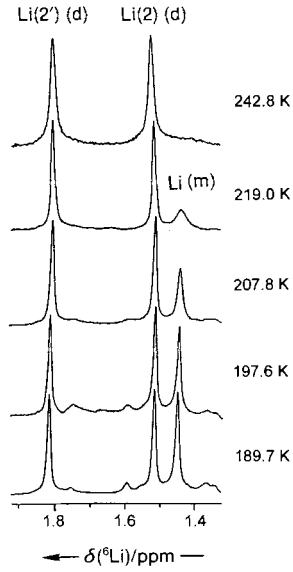


Fig. 14. *Temperature dependence of the $^{6}$Li-NMR spectrum of* **8a** ⇌ **7a** (d = dimer, m = monomer)

On the basis of the negligible activation entropy found for **3**, the dynamic process was attributed to an internal rotation of a monomer subunit within the solvent cage of the dimer [19]. Alternatively, *inter*-aggregate exchange would affect the spectra in the same way, but here solvation of monomeric subunits after dimer dissociation should lead to a large negative activation entropy. In principle, both alternatives could be distinguished by an analysis of the temperature dependence of the $^{13}C,^{6}Li$ spin *m*, because only an *inter*-aggregate process eliminates the $^{13}C,^{6}Li$ coupling, while an *intra*-aggregate process should scramble the spin-spin interactions. In this way, the transition static aggregate – *intra*-aggregate exchange – *inter*-aggregate exchange was detected for the tetramers of *tert*-butyllithium [27] and vinyllithium [28]. In the present case, such an investigation was, however, hampered by the low sensitivity of the $^{13}C$-NMR spectra and the complex structure of the splitting pattern.

It is worth noting that, because of the twofold rotational axis of the substituent, the nonequivalence of the *ortho*-protons in ring A of **7a** at low temperature which results from the chirality of the adjacent cluster can only be explained by a hindered rotation, while the diastereotopicity of the $CH_2$ protons in the Pr groups which has the same origin is not affected by rotations around the C(2)–C(3) bond. *Bauer et al.* [19] assumed for $\mathbf{3}_2$ that rotation of the non-lithiated Ph ring does not take place in the intact dimer, because the measured barrier ($\Delta G^{\neq}(298) = 63.6$ kJ/mol) was much lower than the barrier calculated for Ph-ring rotation by the MNDO method ($\Delta E^{\neq} = 176.6$ kJ/mol). Instead, *intra*-aggregate exchange by '180° rotation of one monomer subunit' causes the interchange. This implies, of course, a relatively high amplitude for torsional vibrations, because a strict rigid orthogonal orientation of the Ph-ring plane with respect to the plane of the double bond is unlikely.

Our results for **7a** support this mechanism, because the coalescence of the $CH_2$ proton signals, which can only result from a rotation of the subunits and not from a hindered rotation around the C(2)–C(3) bond, leads to a barrier which is practically identical with the one found from spectral changes of the Ph protons.

We further note, that in the case of $\mathbf{3}_2$, apparently as a consequence of the different substitution pattern, additional inequivalences were observed for the *meta*-protons and the *ortho*-C-atoms of the non-metalated benzene ring [19], while, in the case of **7a**, these nuclei, at the available field strength, are isochronous over the temperature range studied.

The $^{1}H,^{1}H$-coupling constants of the Pr groups of **7a** estimated from the spectral simulation (*Table 4*) show that the orientation of the alkyl chains in **7a** follows the expectation with a high population of the antiperiplanar conformer **11**.

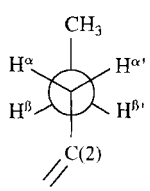


**11**

New aspects related to the structure and the dynamic behavior of dilithiostyrenes of type **1**–**3** are coming from the results obtained for **2**. With respect to the structure, the observation of four different Li-signals at low temperature [24] is most significant. This is the first experimental proof of $C_1$ symmetry for the dimer structure **7**. It verifies theoretical predictions made from MNDO calculations for **3**, where the structure with $C_2$ symmetry was found to be less stable by 19.7 kJ/mol than a distorted structure of lower symmetry. Considering this result, the heteronuclear $^6$Li,$^{13}$C-coupling constants published so far for all dimer systems are most probably still average values. Nevertheless, these parameters seem to vary systematically, with smaller values around 4–5 Hz in the partial dimer structures with identical ligands and larger values of 6–8 Hz in partial structures where the metal bridges an aromatic and an olefinic C-atom.

Aside from the $^{13}$C,$^1$H-coupling constants, a prominent feature of **7b** is the extensive $^6$Li,$^1$H coupling present in this compound which led to the introduction of $^6$Li,$^1$H-shift-correlation experiments [24]. In addition, for the first time, we were able to resolve the homonuclear $^6$Li,$^6$Li coupling in phase-sensitive $^6$Li,$^6$Li-COSY-90 and $^6$Li,$^6$Li-COSY-DQF experiments performed with $^1$H-decoupling. From the cross-peak splitting of the latter, shown in *Fig. 15, a*, a coupling constant of 0.16 Hz was measured. The same result was obtained directly from the 1D INADEQUATE spectrum (*Fig. 7, b*). A more elaborate analysis of this splitting was possible using a treatment developed by *Kim* and *Prestegaard* [29] which yielded in the present case frequency parameters of 0.39 and 0.88 Hz for the absorptive and dispersive INADEQUATE signals from which a splitting of 0.35 Hz and thus a coupling of 0.17 Hz was calculated (*Fig. 15, b*). This analysis was based on the assumption that $J(2',2') \approx J(2',2) \approx J(2,2)$, which seems justified by the small magnitude of the coupling. It means that the $AA'XX'$ system for the dimer can be approximated by an $A_2X_2$ system.

As far as the dynamic behavior is concerned, **7b** forms the most stable dimer of the three dilithiostyrene systems **1**–**3** studied so far. This is true with respect to the *intra*-aggregate exchange as well as to the formation of the monomer. Thus, all measurements for **7b** could be performed at room temperature, while low-temperature work ( < 200 K) was required in the other two cases. Repulsive interactions between the substituents in **7a** and $\mathbf{3}_2$ may be seen to be responsible for the lower barrier to *intra*-aggregate exchange and

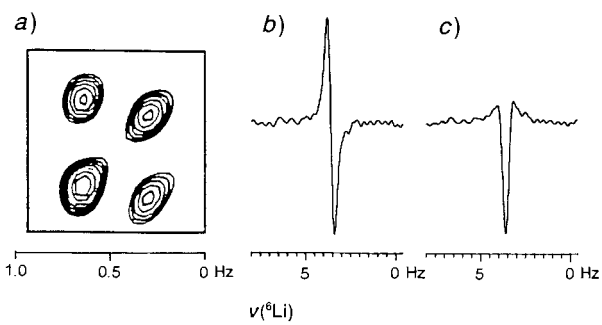


Fig. 15. a) *Cross-peak of the* $^6$*Li,*$^6$*Li-COSY-DQF spectrum of* **7b**; b) *and* c) *absorptive and dispersive line shape of the* $^6$*Li,*$^6$*Li-INADEQUATE signal of* **7b**

dissociation to the monomer, where the loss of the higher coordination energy in the dimer – here each Li-atom has three C-partners – may be compensated for by reduced steric crowding.

Of interest are the significantly different activation parameters found for the coalescence of the $^6$Li-signals in **7a** and $\mathbf{3}_2$ in $Et_2O$ and THF, respectively, on one side and **7b** in glyme on the other. A possible explanation might come from the different solvent properties. The dimer, most probably, is coordinated in glyme with four solvent molecules *via* one MeO group. As a bidendate ligand, glyme might be able to coordinate the adjacent Li-atom with both MeO groups in the transition state during internal rotation of the monomer subunits. This would lower the energy of dissociation to the intimate aggregate of the two monomer subunits in the solvent cage, while at the same time it explains the negative activation entropy due to loss of rotational freedom. In contrast, coordination with monodendate ligands like THF or $Et_2O$ does not change during the rotation process, because solvent molecules from the outer solvent shell will be prevented to penetrate and to solvate the monomeric subunits, because this would lead to solvent-separated dimers and consequently to an *inter*-aggregate exchange. Due to insufficient solvation, the activation energy for the internal-rotation process is higher, while a low activation entropy results.

For the monomer-dimer equilibrium, the dissociation is somewhat less endothermic in the case of **7a** as compared to $\mathbf{3}_2$. Proof of the double Li-bridge in structure **8a** comes from the multiplicity of the $^{13}$C-NMR signals C(2) and C(2′). Both show a *quint.* structure which means coupling to two $^6$Li-nuclei. The assignment of both C-resonances with C(2) at low field was based on increments obtained by comparing the chemical shifts of C(2) and C(2′) in **6** (130.0 and 127.2 ppm, resp.) with those found for ethylene (123.3 ppm [23]), benzene (128.5 ppm [23]), vinyllithium dimer (192.6 ppm [30]), and phenyllithium dimer (188.9 ppm [31]). The predictions are then $\delta(C(2)) = 130.0 + 69.3 = 199.3$ ppm and $\delta(C(2')) = 127.2 + 60.4 = 187.6$ ppm. The best fit with the experimental values is thus found for $\delta(C(2)) = 204.2$ and $\delta(C(2')) = 186.3$ ppm.

Table 5. *Comparison of the $^{13}$C-NMR Chemical-Shift Data* (ppm rel. to $SiMe_4$) *for the Lithiated Aromatic C-Atoms in Phenyllithium Dimer $(PhLi)_2$,* **7a**, **7b**, *and* $\mathbf{3}_2$, *and the Lithiated Olefinic C-Atoms in Vinyllithium Dimer $(CH_2{=}CHLi)_2$,* **7a**, **7b**, *and* $\mathbf{3}_2$

| | $Et_2O$ | $Et_2O$/tmeda | THF | THF/tmeda |
|---|---|---|---|---|
| Lithiated arom. C-atoms | | | | |
| $(PhLi)_2$ | – | 187.3[a]) | 188.9[c]) | – |
| | – | 187.4[b]) | 188.5[d]) | – |
| **7a** | 172.2 | – | 174.0 | – |
| **7b** | 173.1 | – | – | – |
| $\mathbf{3}_2$ | – | | 175.9[e]) | – |
| Lithiated olef. C-atoms | | | | |
| $(CH_2{=}CHLi)_2$ | – | – | 190.8[f]) | 192.6[f]) |
| **7a** | 187.4 | – | – | – |
| **7b** | 177.7 | – | – | |
| $\mathbf{3}_2$ | – | – | 190.2[e]) | |

[a]) [32]. [b]) [30]. [c]) [31]. [d]) [33]. [e]) [19]. [f]) [28].

*Chemical Shifts.* Considering that the dimer structures **7a**, **7b**, and $\mathbf{3}_2$ contain subunits related to phenyl- and vinyllithium dimers, it is of interest to compare the $^{13}$C-NMR chemical shifts for the lithiated C-atoms. The relevant data collected in *Table 5* show that joining the two subunits to the tetralithio cluster results in an upfield shift for the aromatic C-atoms of *ca.* 14 ppm. A similar shielding is found for the olefinic C-atom by comparing data for vinyllithium with those for **7b** ($\Delta\delta = -13.9$ ppm) and for **7a** and $\mathbf{3}_2$, after allowance for a low-field shift caused by an $\alpha$-effect of the substituents at C(2) (9.1 ppm [23]) has been made ($\Delta\delta = -10.9$ ppm). This conforms with the general finding that higher aggregation of organolithium compounds is associated with high-field shifts for the lithiated C-atoms [33].

A final comment concerns the $^1$H-NMR chemical shifts of the Ph protons in **6** where a puzzling difference exists between the well-resolved resonances of ring A and the nearly degenerate resonances of ring B. It is tempting to assign this difference to conformational effects, but a force-field calculation with the MM2 method [34] showed nearly identical rotational angles between the planes of each of the two Ph rings and the plane of the double bond (*ca.* 20°). Thus, it appears that diamagnetic anisotropy effects of the C,C and C,H bonds and/or *van-der-Waals* effects of the vicinal Pr group are the cause of the larger chemical-shift differences in ring A. That indeed a mutual interaction of the vicinal substituents occurs is born out by the $^{13}$C-NMR chemical shifts of the Ph C-atoms (*Table 2*), which differ in the *ipso*- and for the *ortho*-positions, while those of the *meta*- and *para*-positions are practically identical. For C(1″), we find a high-field of 2.54 ppm which can be explained as a vicinal $\gamma$-effect. The opposite is found for C(2″,6″), which are deshielded by 2.76 ppm relative to C(2′,6′).

## Experimental Part

*Compounds.* Dilithio derivatives **1** and **2** were synthesized as described [16a] [17] and transferred to 5-mm (o. d.) NMR tubes which were sealed after addition of the solvent. Sample concentrations were 0.2M in $(D_{10})Et_2O$ and 0.4M for **1** in THF. For $^6$Li-isotopic enrichment (*ca.* 96%), $^6$Li-powder was prepared [35] from commercial $^6$Li-metal (*Aldrich*). All operations were performed under dry Ar, solvents were dried over Na/K alloy. An authentic sample of **6** [36] (b.p. 120°/0.1 Torr, $^1$H-NMR as described [37]) was synthesized according to [37]. The synthesis of **9** followed the standard procedure [16a], but with $C_6D_5MgBr$, prepared from bromo($D_5$)benzene [33], as deuteriation synthon; **10** was derived from **5** by *o*-lithiation and subsequent deuterolysis [17].

*Spectra.* NMR Measurements were performed with a *Bruker-AMX-FT-NMR* spectrometer operating at 400.13 MHz for $^1$H, 100.61 MHz for $^{13}$C, 58.88 MHz for $^6$Li, and 144.5 MHz for $^7$Li and equipped with an *Aspect-32* computer and the *Bruker* variable-temp. unit. Broadband multinuclear probeheads for direct and inverse measurements and a $^2$H lock system were used. Temp. measurements were performed with the methanol thermometer [38]; $\delta$-values given in the *Figures* are relative to $SiMe_4$ (internal, $^1$H, $^{13}$C) or 0.1M LiBr in THF (external, $^6$Li).

Two-dimensional experiments were performed using standard *Bruker* software. Spectral parameters and most significant cross-peaks, if not given in the *Figures*, are listed as follows: *Analysis of* **6**: $^1$H,$^1$H-NOESY spectrum, sweep width (*SW*) 3012 Hz, 128 $t_1$ experiments of 32 transients, mixing time 1 s with 20% statistical variation to eliminate COSY signals, relaxation delay (*RD*) 7 s, exper. time 10.5 h; HETCOR spectrum (*Fig. 4*) *SW*1 ($^1$H) 120 Hz, *SW*2 ($^{13}$C) 3268 Hz, 128 $t_1$ increments of 64 transients, *RD* 3.5 s, exper. time 8.6 h. *Spectral assignment of* **1**: COSY-45 exper. at 298 K, *SW* 914 Hz, 128 $t_1$ experiments of 16 transients, exper. time 2.1 h, cross-peaks: H–C(3′)/H–C(4′), H–C(5′)/H–C(6′); $^1$H,$^1$H-NOESY at 298 K, *SW* 3164 Hz, 128 $t_1$ experiments of 32 transients, mixing time 0.7 s ± 20%, *RD* 6 s, exper. time 9.9 h; cross-peaks: H–C(2″,6″)/$CH_2$(3); $^{13}$C,$^1$H-INEPT-based shift correlation at 298 K, *SW*1 1572 Hz, *SW*2 4829 Hz, 64 $t_1$ experiments of 256 transients, *RD* 2 s, exper. time 10.5 h; one-bond cross-peaks for all CH moieties; inverse long-range $^{13}$C,$^1$H correlation at 298 K: *SW*1 3846 Hz, *SW*2

3164 Hz, 128 $t_1$ experiments of 208 transients, $\Delta$ delay 125 ms (optimized for $J(^{13}C,^{1}H) = 0.8$ Hz), *RD* 2 s, exper. time 5.7 h; cross-peaks: C(1″)/*H*–C(3″,5″), C(1)/*H*–C(6′), C(1′)/*H*–C(3′), C(1′)/*H*–C(5′), C(2′)/*H*–C(4′); HOESY spectrum (*Fig. 6b*) *SW*1 ($^{1}$H) 4 kHz, *SW*2 ($^{6}$Li) 80 Hz; 256 $t_1$ increments, mixing time 1 s, *RD* 1 s, exper. time 13 h. *Spectral assignment for* **2**: COSY-90 spectrum: *SW*(1,2) 1 kHz, 256 $t_1$ experiments of 16 transients, *RD* 2 s, exper. time 3.5 h; cross-peaks for all vicinal $^{1}$H nuclei; $^{13}$C,$^{1}$H-HSC (inverse INEPT-based) experiments: *SW*1 4 kHz, *SW*2 7.5 kHz, 128 $t_1$ experiments of 256 transients, $\Delta$ delays 3.3 ms (optimized for $J(^{13}C,^{1}H) = 150$ Hz), exper. time 19.5 h; cross-peaks for all CH moieties; $^{13}$C,$^{1}$H-HMBC experiment (phase sensitive): *SW*1 6.8 kHz, *SW*2 1 kHz, 128 $t_1$ experiments of 16 transients, *D* 96.5 ms (optimized for $J(^{13}C,^{1}H) = 5.5$ Hz), *RD* 1 s, exper. time

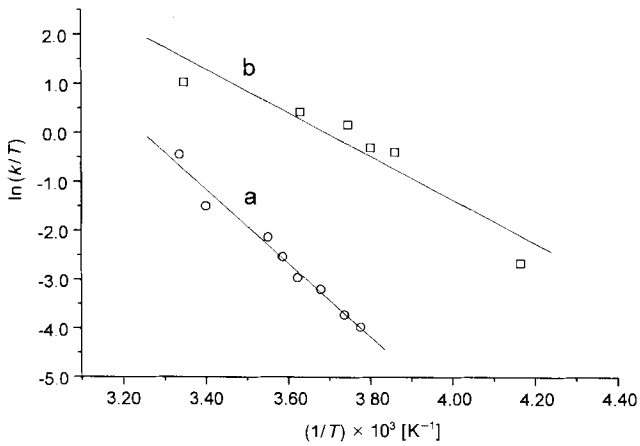


Fig. 16. Eyring *diagrams for the rate constants extracted from the line-shape analysis of the* $^{6}$*Li-NMR spectra of* **7a** (a) *and* **7b** (b)

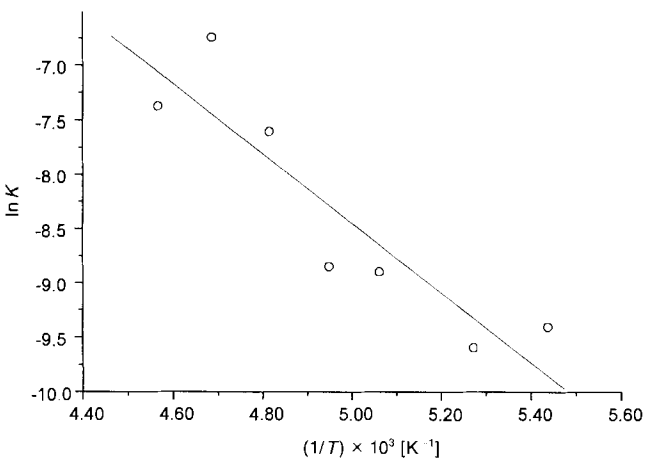


Fig. 17. van't Hoff *diagram for the monomer-dimer equilibrium* **8a**⇌**7a**

7 h; cross-peaks: C(1)/*H*–C(6'), *C*(1')/*H*–C(5'). *INADEQUATE Spectra* (*Fig. 7*): for **1**, spectral window 147 Hz, $1/4J = 0.78$ s according to a line splitting of 0.32 Hz due to $^6$Li,$^6$Li coupling; for **2**, spectral window 70 Hz, $1/4J = 0.78$ s as before.

The $^6$Li line-shape analysis of the $^6$Li-spectra for **7a** (*Fig. 12*) was based on the modified *Bloch* equations [23] [26] and exper. and calc. spectra (PC program LINESHAPE [39]) were matched by visual comparison through changes in the chemical-shift difference $\delta\nu$, the natural line width, and the rate constant. The following data ($k/s^{-1}$ (*T*)) were obtained: 192.3 (299.7); 65.8 (294.1); 33.3 (281.6); 22.2 (278.8); 14.3 (276.0); 11.1 (271.8); 6.5 (264.8). The *Eyring* diagram is shown in *Fig. 16*. 2D Exchange spectra yielded similar values: 3.0 (264.6); 0.14 (243.7); 0.1 (231.9); 0.05 (224.1); 0.01 (209.7). Due to the low signal/noise ratio, 2D peak integration was difficult, and these results were not included in the least-square analysis.

The thermodynamic parameters for the dimer-monomer equilibrium of **1** in THF/tmeda were derived from the integration of the $^6$Li-NMR spectra (*Fig. 14*). Concentrations were calculated from the signal integrals and based on the sample concentration (mol $l^{-1}$) and the sample volume where the temp. variation of the THF density was taken into account [19]. The well separated low-field signal was used to determine the concentration of **7a**. This intensity was substracted from the integral of the partially overlapping high-field signals to obtain the concentration of the monomer **8a**. The following results (*T*, [**8a**], [**7a**], $K \cdot 10^5$) were obtained: 184 K, 0.270, 0.090, 8.3; 189.7 K, 0.274, 0.088, 6.8; 197.6 K, 0.251, 0.097, 13.7; 202.1 K, 0.248, 0.097, 14.4; 207.7 K, 0.207, 0.116, 49.9; 213.4 K, 0.177, 0.129, 117.9; 219.0 K, 0.196, 0.119, 63.0. The *vant' Hoff* plot is shown in *Fig. 17*.

For **7b** (in glyme), the line-shape analysis of the $^6$Li spectra (*Fig. 13*) yielded $k/s^{-1}$ (*T*) = 833.3 (298.8); 416.6 (275.5); 312.5 (266.9); 192.3 (263.0); 172.4 (258.9); 16.6 (240.0). The *Eyring* diagram is shown in *Fig. 16*.

We are indebted to Dipl.-Chem. *A. Focke* for providing the spectra of *Fig. 1* and to cand. chem. *Th. W. Gross* for the synthesis of **6**. Financial support by the *Deutsche Forschungsgemeinschaft* and the *Fonds der Chemischen Industrie* is gratefully acknowledged.

## REFERENCES

[1] W. Baumann, Y. Oprunenko, H. Günther, *Z. Naturforsch., A: Phys. Sci.* **1995,** *50,* 429.
[2] H. Günther, D. Moskau, D. Schmalz, *Angew. Chem.* **1987,** *99,* 1242; *ibid. Int. Ed.* **1987,** *26,* 1212.
[3] R. D. Thomas, in 'Isotopes in the Physical and Biomedical Sciences', Eds. E. Buncel and J. R. Jones, Elsevier, Amsterdam, 1991, Chapt. 7.
[4] W. Bauer, P. v. R. Schleyer, in 'Advances in Carbanion Chemistry', Ed. V. Snieckus, Jai Press, Greenwich, Connecticut, 1992, p. 89.
[5] D. B. Collum, *Acc. Chem. Res.* **1993,** *26,* 227.
[6] H. Günther, 'Encycl. NMR', Wiley, to be published.
[7] O. Eppers, H. Günther, *Tetrahedron Lett.* **1989,** *30,* 6155.
[8] R. D. Thomas, D. H. Ellington, *Magn. Reson. Chem.* **1989,** *27,* 628.
[9] A. G. Avent, C. Eaborn, M. N. A. El-Kheli, M. E. Molla, J. D. Smith, A. C. Sullivan, *J. Am. Chem. Soc.* **1986,** *108,* 3854.
[10] W. Bauer, G. Müller, R. Pi, P. v. R. Schleyer, *Angew. Chem.* **1986,** *98,* 1130; *ibid. Int. Ed.* **1986,** *25,* 1103.
[11] H. Günther, D. Moskau, R. Dujardin, A. Maercker, *Tetrahedron Lett.* **1986,** *27,* 2251.
[12] D. Moskau, F. Brauers, H. Günther, A. Maercker, *J. Am. Chem. Soc.* **1987,** *109,* 5532.
[13] D. Moskau, W. Frankmölle, O. Eppers, H.-E. Mons, H. Günther, *Proc. Indian Acad. Sci. (Chem. Sci.)* **1994,** *106,* 1471.
[14] L. D. Field, M. G. Gardiner, C. H. L. Kennard, B. A. Messerle, C. L. Raston, *Organometallics* **1991,** *10,* 3167.
[15] O. Eppers, H. Günther, *Helv. Chim. Acta* **1990,** *73,* 2071.
[16] a) A. Maercker, K.-D. Klein, *J. Organomet. Chem.* **1991,** *401,* C1; b) O. Eppers, H. Günther, K.-D. Klein, A. Maercker, *Magn. Reson. Chem.* **1991,** *29,* 1065; c) K.-D. Klein, Ph. D. Thesis, University of Siegen, 1990.
[17] A. Maercker, H. Bodenstedt, L. Brandsma, *Angew. Chem.* **1992,** *104,* 1387; *ibid. Int. Ed.* **1992,** *31,* 1339.

[18] J.E. Mulvaney, Z.G. Garlund, S.L. Garlund, *J. Am. Chem. Soc.* **1963,** *85,* 3897; J.E. Mulvaney, Z.G. Garlund, S.L. Garlund, D.J. Newton, *ibid.* **1966,** *88,* 476.
[19] W. Bauer, M. Feigel, G. Müller, P. v. R. Schleyer, *J. Am. Chem. Soc.* **1988,** *110,* 6033.
[20] *A. Maercker et al.*, unpublished.
[21] A.J. Ashe III, P.M. Savla, *J. Organomet. Chem.* **1993,** *461,* 1.
[22] J. Jeener, B.H. Meier, P. Bachmann, R.R. Ernst, *J. Chem. Phys.* **1979,** *71,* 4546; for reviews see: R. Willem, *Progr. NMR Spectrosc.* **1987,** *20,* 1; C.L. Perrin, T.J. Dwyer, *Chem. Rev.* **1990,** *90,* 935.
[23] See H. Günther, 'NMR-Spektroskopie', 3rd edn., Thieme, Stuttgart, 1993; 'NMR Spectroscopy', 2nd edn., Wiley, Chichester, 1995.
[24] H.-E. Mons, H. Günther, A. Maercker, *Chem. Ber.* **1993,** *126,* 2747.
[25] O. Eppers, Th. Fox, H. Günther, *Helv. Chim. Acta* **1992,** *75,* 883.
[26] H.S. Gutowsky, R. Holm, *J. Chem. Phys.* **1956,** *25,* 1228; see also J. Sandström, 'Dynamic NMR Spectroscopy', Academic Press, London, 1982.
[27] R.D. Thomas, M.T. Clarke, R.M. Jensen, T.C. Young, *Organometallics* **1986,** *5,* 1851.
[28] W. Bauer, C. Griesinger, *J. Am. Chem. Soc.* **1993,** *115,* 10871.
[29] Y. Kim, J.H. Prestegaard, *J. Magn. Reson.* **1989,** *84,* 9.
[30] G. Fraenkel, H. Hsu, B.M. Su, in 'Lithium, Current Applications in Science, Medicine, and Technology', Ed. R.O. Bach, Wiley, New York, 1985, Chapt. 19; Hsi-Pai Hsu, Ph.D. Thesis, Ohio State University, 1983.
[31] D. Seebach, R. Hässig, J. Gabriel, *Helv. Chim. Acta* **1983,** *66,* 308.
[32] O. Eppers, H. Günther, *Helv. Chim. Acta* **1992,** *75,* 2553.
[33] W. Bauer, W.R. Winchester, P. v. R. Schleyer, *Organometallics* **1987,** *6,* 2371.
[34] N.L. Allinger, *J. Am. Chem. Soc.* **1977,** *99,* 8127; U. Burkert, N.L. Allinger, 'Molecular Mechanics', ACS Monograph No. 177, American Chemical Society, Washington, D.C., 1982.
[35] A. Maercker, M. Theis, *Organomet. Synth.* **1986,** *3,* 378.
[36] A. Jung, M. Brini, *Bull. Soc. Chim. Fr.* **1964,** 693.
[37] A. Maercker, *Liebigs Ann. Chem.* **1970,** *732,* 151.
[38] A.L. van Geet, *Anal. Chem.* **1970,** *42,* 679.
[39] H. Günther, unpublished.